

Title	3D open-worked inverse opal TiO <sub>2</sub> and GeO <sub>2</sub> materials for long life, high capacity Li-ion battery anodes
Authors	McNulty, David;Lonergan, Alex;O'Hanlon, Sally;O'Dwyer, Colm
Publication date	2017-10-18
Original Citation	McNulty, D., Lonergan, A., O'Hanlon, S. and O'Dwyer, C. (2018) '3D open-worked inverse opal TiO <sub>2</sub> and GeO <sub>2</sub> materials for long life, high capacity Li-ion battery anodes', Solid State Ionics, 314, pp. 195-203. doi: 10.1016/j.ssi.2017.10.008
Type of publication	Article (peer-reviewed)
Link to publisher's version	<a href="http://www.sciencedirect.com/science/article/pii/S0167273817307312">http://www.sciencedirect.com/science/article/pii/S0167273817307312</a> - 10.1016/j.ssi.2017.10.008
Rights	© 2017 Elsevier B.V. All rights reserved. This manuscript version is made available under the CC-BY-NC-ND 4.0 license. - <a href="http://creativecommons.org/licenses/by-nc-nd/4.0/">http://creativecommons.org/licenses/by-nc-nd/4.0/</a>
Download date	2025-07-04 00:02:41
Item downloaded from	<a href="https://hdl.handle.net/10468/5867">https://hdl.handle.net/10468/5867</a>



# UCC

**University College Cork, Ireland**  
Coláiste na hOllscoile Corcaigh

# 3D Open-worked Inverse Opal TiO<sub>2</sub> and GeO<sub>2</sub> Materials for Long Life, High Capacity Li-ion Battery

## Anodes

David McNulty<sup>a</sup>, Alex Lonergan<sup>a</sup>, Sally O'Hanlon<sup>a</sup>, and Colm O'Dwyer<sup>a,b,\*</sup>

<sup>a</sup> *School of Chemistry, University College Cork, Cork T12 YN60, Ireland*

<sup>b</sup> *Micro-Nano Systems Centre, Tyndall National Institute, Lee Maltings, Cork T12 R5CP, Ireland*

**Keywords:** TiO<sub>2</sub>, GeO<sub>2</sub>, Inverse Opal, Li-ion, Semiconductor, Anode, Nanomaterials

\*E-mail: [c.odwyer@ucc.ie](mailto:c.odwyer@ucc.ie), Tel: +353 21 490 2732.

## Abstract

In this short review, we overview some advancements made in Li-ion battery anode development, where the structural arrangement of the material plays an important role. Specifically, we summarise the benefits of 3D macroporous structure imposed the anode material, in order to improve ionic and electronic conductivity in the absence of conductive additives and binders. Two anode materials are overviewed: TiO<sub>2</sub> and GeO<sub>2</sub>. These are either high capacity anode materials or accessible, abundant materials that are capable of very stable and long-term cycling. We have focused this review on 3D inverse opal structures of these anodes and summarise their enhanced behaviour by comparing their performance metrics to a wide range of nanoscale and porous analogues of these materials.

## Introduction

The market for Li-ion batteries for consumer electronics and related items is expected to soar by a factor of more than 60 between 2012 and 2020, rising to \$3.6bn a year according to a new report from research firm HIS and others. [1, 2] Underlying almost all Li-ion batteries are basic challenges [3-5] concerning the materials that are used. [6] Researchers [7, 8], including our group [9, 10], have identified materials that can store more energy than conventional technology [11], but the material swells significantly when fully charged then shrinks again during discharge. [4, 12] This swelling and shrinking quickly breaks down the electrical contacts in some materials, contributing to capacity fading, reduction in voltage and energy. Our approach, in tandem with many other approaches worldwide, [13] is to advance the use of hierarchical, ordered porous materials [14-16] whose crystal structure is designed to remove heterogeneities in volume changes throughout the material, and increase energy density to offset lower volumetric energy density. Importantly, electrical conductivity is not adversely affected and long-term cycling is very stable.

Electrode materials for Li-ion batteries store electrochemical charge by intercalating lithium ions into the lattices of crystalline solids and into disordered vacancies within amorphous hosts. New materials on the nanoscale tackle the slow kinetics of solid-state ion diffusion into bulk electrode materials and have improved capacity retention. Essentially, these limits on ionic mobility are at least partially overcome by fabricating battery components that have solid-state ion diffusion path lengths on a nanometer-length scale. We recently surveyed many promising materials and nanoscale sizes for emerging battery constructs, and engineering material structure from the atomic scale to the electrode scale are crucial for future advances in energy storage [10, 17]. In batteries, separate conductive additives and binders etc. add significant 'dead weight'. To get a high volume fraction of nanostructured active material on a surface with efficient ion and electron pathways, reducing the complexity and additives within the random network of active material is required. To do this, we can remove conductive additives such as carbons, and non-recyclable polymeric binders used stitch all materials together as the electrode slurry, to improve the gravimetric energy density of active material. This helps to regain some gravimetric capacity losses caused by the multi-functional porosity. An ordered, porous material can potentially allow fast charging and alleviate material breakup during many charge cycles.

The ordered porous 3D material architecture provides definable short electron and ion transport lengths in the active material and electrolyte (yielding high-power density) while maintaining a high volume of active material (maintaining high-energy density). [14, 18, 19] Rates from several hundred C up to 1000C (~ 4 s) for lithium-ion chemistries could potentially be achieved, enabling fabrication of a lithium-ion material that can be fully charged in a matter of minutes or seconds. Nanotechnology together with carbon coating has provided some possibilities for these requirements in standard battery architectures. [20, 21] Inverse opals and other nanomaterials have successfully improved the power density of lithium-ion electrodes when used in powder form.

With respect to inverse opals, three-dimensionally interconnected macropores facilitate the rapid flux of liquid electrolyte solutions, such that several hundred  $\text{m}^2 \text{g}^{-1}$  of electrode interfaces are simultaneously accessible to lithium or other mobile ionic charges. This degree of macropore interconnectivity is intentionally tailored from self-assembled close-packed templates [22]. For example, the ionic conductivity of a 1 M  $\text{LiPF}_6$  liquid electrolyte solution is only impeded by a factor of two when ion transport occurs through the interconnected macropores of monolithic carbon inverse opals (electrode thicknesses: 300  $\mu\text{m}$ –3 mm). For these materials, fast transport kinetics have been achieved in one dimensional (1D) carbon nanotube- and two dimensional (2D) graphene nanosheet-based hybrid electrodes. [23] However in 1D and 2D electrodes, the fast electron transport is restricted at least in one dimension because of the structural anisotropy of the electrodes. [24, 25] As a result, that dimension constrains the ambipolar (ionic and electronic) diffusion, eventually slowing down the transport kinetics in the entire battery. Such kinetics problems become more severe at high current densities (rates).

Macroporous lithium ion electrodes methods developed fabricated by Stein [26-30] and Dunn [31] over two decades ago by means of colloid templating, reduce the ion transport length and are particularly promising. However, the relatively low electrical conductivity of the macroporous host can limit the rate performance; changes to the very material as well as its structuring are also needed. Several excellent reviews and key reports summarizing scientific and performance indicators for Li-ion electrode materials templated with colloidal crystals are available. [32-34].

In this short review, we summarise the most recent advances in binder-free, conductive additive-free, structured porous inverse opal anodes materials for Li- ion batteries. We survey TiO<sub>2</sub> and GeO<sub>2</sub> materials and compare some of the promising performance metrics of these materials in terms of specific capacity and long cycle life.

## **TiO<sub>2</sub> Anode Materials**

In recent years, titanium dioxide (TiO<sub>2</sub>) has been the subject of a tremendous research effort due to its unique properties such as low environmental impact and cost, safety, and stability which make it useful for a wide range of applications including photocatalysis[35, 36], sensors[37, 38], drug delivery and energy storage. [39-42] Consequently, a great number of TiO<sub>2</sub> based nanostructures have been reported over the last decade such as nanowires, nanorods, nanoparticles and nanoflowers. [43-46] TiO<sub>2</sub> has also attracted a lot of attention as an intercalation mode anode material for Li-ion batteries, being a low voltage insertion host for Li<sup>+</sup> and as a fast Li<sup>+</sup> insertion/removal host. [47, 48] Anatase, rutile, and TiO<sub>2</sub>(B) with varying nanostructure architectures have been investigated as anode materials for lithium ion batteries. [49-51] Previous reports have indicated that TiO<sub>2</sub> nanostructures demonstrate poor performance at high rates as well as poor long-term cycling performance due to issues including the inherent low conductivity of semiconducting TiO<sub>2</sub> materials and volume changes associated with the insertion and removal of Li<sup>+</sup>. [52-55] To improve the electrochemical performance of TiO<sub>2</sub> anode materials there have been many reports on the combination of TiO<sub>2</sub> with highly conductive materials such as composites with carbon nanotubes (CNTs) or graphene and the coating of TiO<sub>2</sub> nanostructures with graphitic carbon. [52, 56, 57] However the TiO<sub>2</sub> component of composites still suffer from volume expansion during cycling, resulting in capacity fading issues overtime and for the carbon coated samples, any uncoated areas remain vulnerable with low conductivity. [58]

Recently, inverse opal (IO) structures have emerged as a promising architecture for high performance Li-ion cathode and anode materials due their numerous inherent advantageous properties, some of which are summarised schematically in Fig. 1(a,b). [59-63] IOs represent a high surface area, highly ordered, porous, 3D interconnected network of material which may remove the necessity for binders and conductive additives. [64-66] There are few papers investigating the electrochemical performance of anatase and rutile TiO<sub>2</sub> IO

structured anode materials, with one of the first reports being from Kavan et al. in 2004. [67] Anatase IOs were prepared via infilling of a latex sphere template with various Ti containing precursors. It was reported that the anatase IOs demonstrated sluggish electrochemical performance for  $\text{Li}^+$  insertion compared to non-templated anatase samples. It was suggested that the worsened performance was due to poor electrical contacts between the particles in the extremely open nano crystalline IO network. This is the only report suggesting that the IO structure was detrimental to the electrochemical performance of  $\text{TiO}_2$  and in recent years the benefits of  $\text{TiO}_2$  IOs have been demonstrated through the efforts of various research groups. One aspect of inverse opal electrode materials that is critical, is the quality of the adhesion to the current collector. This is important of course is flooded cells where the electrode is immersed in excess electrolyte. In coin cells, where the electrode is flat and material cannot fall off under gravity in solution, the method of cells sealing and crimping of button cells is very important. In our survey of the literature of porous materials for Li-ion batteries in non-composited of slurried form, reported performances are assumed to be free of issues associated with changes to material adhesion after cell assembly.

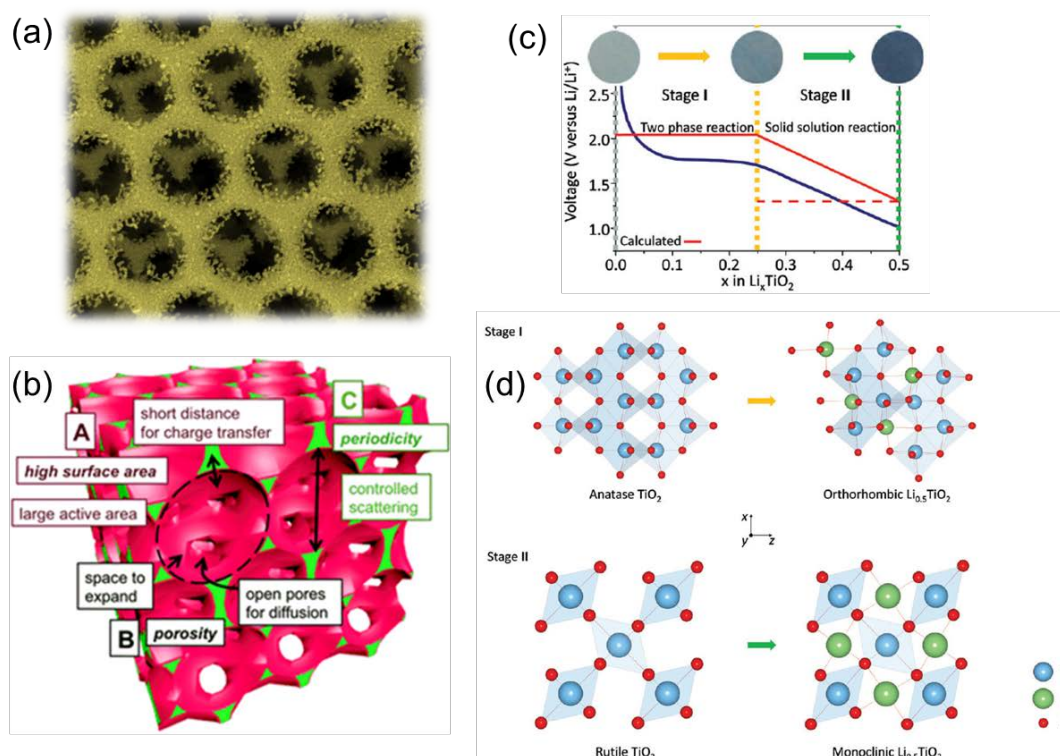


**Fig. 1.** (a) Typical morphology of an inverse opal metal oxide, formed from an inverse replica of a colloidal opal template. (b) Schematic representation highlighting beneficial features of a 3D macroporous interconnected active materials. (c) Measured and calculated charge profile (anode) for mixed anatase/rutile ordered porous nanotube layer material showing two regions associated with intercalation and solid solution reactions with lithium as a function of Li mole fraction [64]. (d) Summary of Li-induced phase changes from tetragonal anatase and rutile  $\text{TiO}_2$ , reproduced from Ref. [64].

Accurate control in synthesis or preparation of  $\text{TiO}_2$  materials for Li-ion battery anode is important due to the differences in Li reactions with  $\text{TiO}_2$  polymorphs. The anatase and rutile phases undergo two-phase and solid solution reactions, respectively, and do so with specific mole fractions of reacted lithium [68]. Fig. 1(c,d), reproduced from Ref. [69], shows the nature of lithium reaction with each phase, and notably, significantly different voltages vs. Li are characteristics of anatase compared to rutile  $\text{TiO}_2$ , even when rutile  $\text{TiO}_2$ . Typically, the reaction steps of  $\text{TiO}_2$  polymorphs with lithium includes a tetragonal anatase to orthorhombic  $\text{Li}_{0.5}\text{TiO}_2$  transition, whereas rutile  $\text{TiO}_2$  converts to a monoclinic  $\text{P2/m}$  space group for  $\text{Li}_{0.5}\text{TiO}_2$ ). What is notable about this phase, is that at a lower voltage, there is an extended solid solution region up to a lithium mole fraction of  $x = 0.5$ . In this solid solution limit, charge-discharge reversibility is efficient, and mitigate sluggish kinetics of Li diffusivity.

The electrochemical performance of anatase  $\text{TiO}_2$  IOs was revisited by Kim et al. in 2012. [70] Anatase IOs were prepared via infilling of a polystyrene sphere (PS) template with a solution of titanium (IV) ethoxide in ethanol. The effect of C-rate on the initial charge capacity was investigated, with initial capacities of  $\sim 360$ , 150 and 110 mAh/g being achieved when charged using C-rates of 0.05, 5 and 30 C, respectively. The first long term cycling of anatase  $\text{TiO}_2$  IOs was reported by Jiang et al. in 2013. [71] Three-dimensionally quasi-ordered macroporous  $\text{TiO}_2$  samples were prepared via infilling of a poly(vinyl alcohol) (PVA) gelled crystalline colloidal array (GCCA) with a titanium tetrabutoxide precursor solution, as shown in Fig. 2k. Capacity values of  $\sim 125$  and 120 mAh/g were reported after the 100<sup>th</sup> and 200<sup>th</sup> cycles when cycled using a specific current of 400 mA/g. Jin et al. prepared anatase  $\text{TiO}_2$  IOs via infilling of a poly(styrene-methyl methacrylate-3-sulfopropyl methacrylate, potassium salt) (P(St-MMA-SPMAP)) sphere template with a solution of  $\text{TiCl}_4$  in ethanol. [72] The resulting anatase  $\text{TiO}_2$  IOs (shown in Fig. 2j) were cycled using a C-rate of 1 C and demonstrated reversible capacities of  $\sim 130$  and 125 mAh/g after the 100<sup>th</sup> and 200<sup>th</sup> cycle which are quite similar to the values reported by Jiang et al. The exceptional capacity retention properties of anatase  $\text{TiO}_2$  IOs prepared on carbon cloth were reported by Lui et al. [73] Carbon cloth was first dipped into a suspension of PS and then this sphere coated carbon cloth was immersed in a sol-gel solution consisting of ethanol, hydrochloric acid, and titanium butoxide prior to thermal treatment. The anatase IOs formed in this

manner, which are shown in Fig. 2l, demonstrated impressive capacity values, exhibiting capacities of ~ 135, 133 and 110 mAh/g after the 100<sup>th</sup>, 200<sup>th</sup> and 1000<sup>th</sup> cycle.

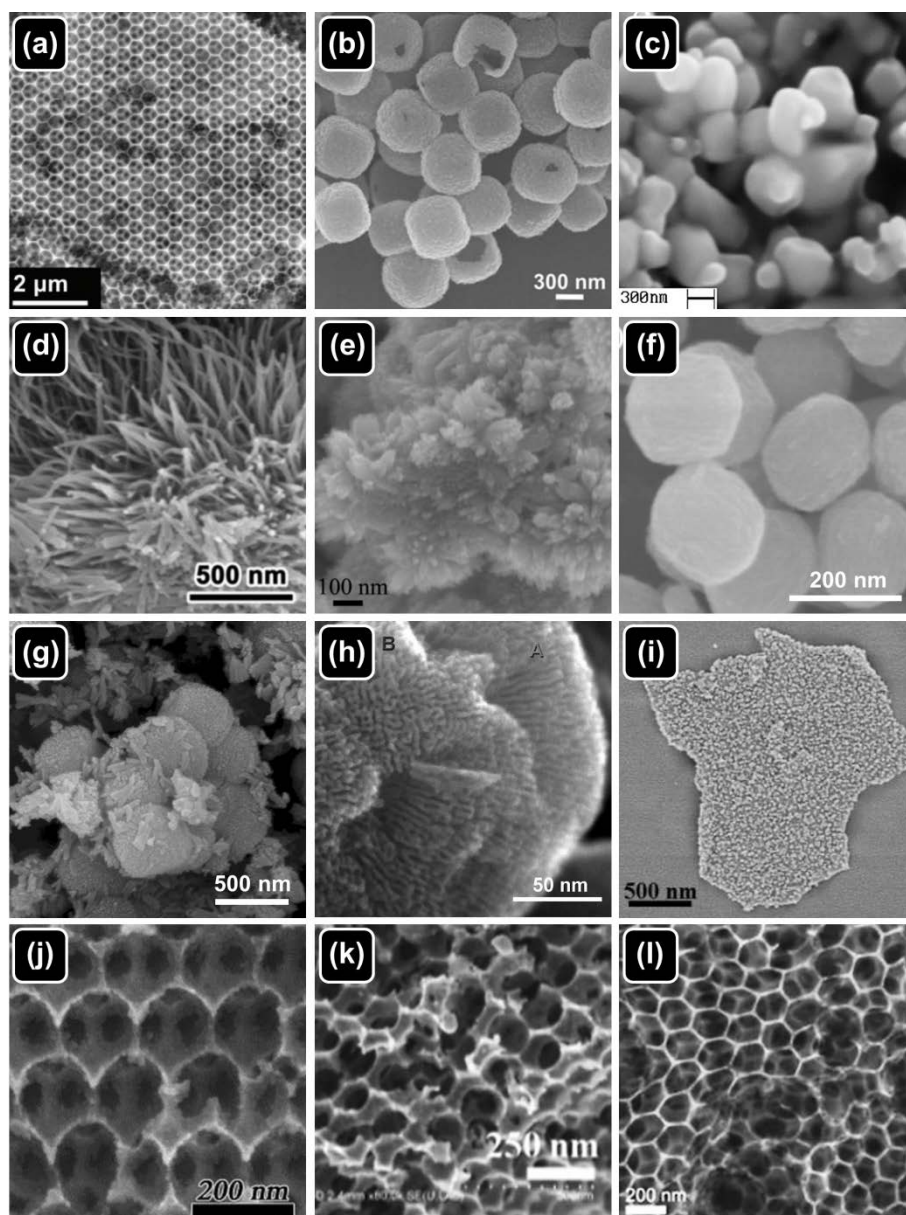


**Fig. 2.** SEM images of (a) TiO<sub>2</sub> inverse opal [69], (b) TiO<sub>2</sub> submicroboxes [46], (c) nanosized TiO<sub>2</sub> [71], (d) TiO<sub>2</sub> nanoneedles [72], (e) TiO<sub>2</sub> nanorods [73], (f) TiO<sub>2</sub> mesocrystals [74], (g) nanosized TiO<sub>2</sub> [75], (h) mesoporous TiO<sub>2</sub> [76], (i) TiO<sub>2</sub> nanocrystals [770], (j) TiO<sub>2</sub> IO [67], (k) TiO<sub>2</sub> IO [66] and (l) TiO<sub>2</sub> IO [68].

Recently, there has also been a report on the electrochemical performance of rutile TiO<sub>2</sub> IOs as an anode material. [74] This crystal structure is the naturally occurring polymorph of TiO<sub>2</sub> in the earth, yet proves to be elusive in many of the simpler synthesis of nanoscale TiO<sub>2</sub>. Some approaches facilitate recrystallization to rutile phase, but limited studies reported direct and stable rutile phase formation, especially uniphasic form through all the material or powder. Often, mixed anatase and rutile TiO<sub>2</sub> can form [75], even from oxidation

of metallic titanium strips (for TiO<sub>2</sub> nanotube layers)[69], or from random mixtures of crystal sizes in large-scale powder synthesis methods including spray pyrolysis.

IO samples were prepared by infilling of a PS template with a TiCl<sub>4</sub>·2THF precursor solution, as illustrated in Fig. 3a. Thermal treatment of the infilled templates resulted in the decomposition of the sacrificial PS template and the formation of a highly porous crystalline IO network with pore sizes of ~ 400 nm, as shown in Fig. 2a and 3b. Rutile TiO<sub>2</sub> IOs demonstrated exceptional capacity retention achieving specific capacities of ~ 170 and 140 mAh/g after the 100th and 1000th cycles respectively, at a specific current of 75 mA/g, as can be seen in Fig. 3d. This corresponded to a capacity retention of ~ 82.4% between the 100<sup>th</sup> and 1000<sup>th</sup> cycles. From the rate capability test in Fig. 3e, it is clear that the rutile TiO<sub>2</sub> IO materials demonstrated significant reversible capacity, considerable capacity retention and outstanding rate performance, when cycled using a series of increasing specific currents. The long-term cycle life performance of the rutile TiO<sub>2</sub> IO samples was further investigated by cycling a sample 5000 times using a specific current of 450 mA/g, as shown in Fig. 3f. The gradual decrease in the capacity values resulted in charge capacities of ~ 103 and 76 mAh/g after 1000 and 5000 cycles, respectively. This corresponds to only a ~ 26% loss in capacity between the 1000<sup>th</sup> and 5000<sup>th</sup> cycles, again demonstrating the impressive stability of the TiO<sub>2</sub> IO structure, particularly when cycled using a large specific current.

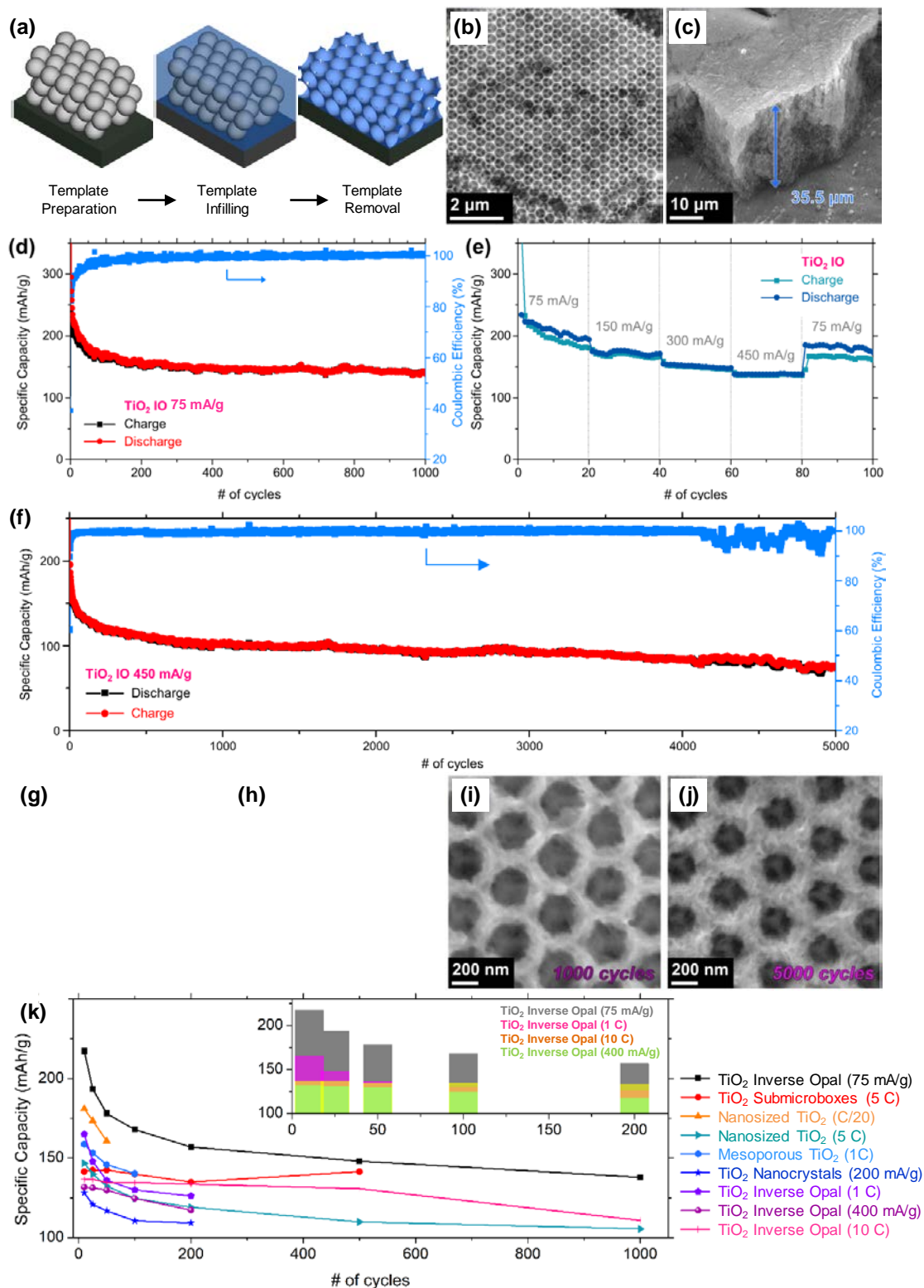


**Fig. 3.** (a) Schematic representation of the preparation procedure for rutile  $\text{TiO}_2$  IO materials. (b) and (c) SEM images of a typical rutile  $\text{TiO}_2$  IO sample. (d) Specific capacity and coulombic efficiency values obtained for  $\text{TiO}_2$  IO over 1000 cycles, at a specific current of 75 mA/g in a potential window of 3.0 – 1.0 V (vs  $\text{Li}/\text{Li}^+$ ). (e) Rate capability test for  $\text{TiO}_2$  IO over 100 cycles, using specific currents ranging from 75 to 450 mA/g. SEM images of (g) an as-prepared  $\text{TiO}_2$  IO sample and IO samples after (h) 100, (i) 1000 and (j) 5000 cycles. (k) Comparison of reported specific capacity values for select  $\text{TiO}_2$  nanostructures:  $\text{TiO}_2$  IO (75 mA/g rate) [74],  $\text{TiO}_2$  submicroboxes [51], nanosized  $\text{TiO}_2$  [76],  $\text{TiO}_2$  nanoneedles (see Table 1) [77],  $\text{TiO}_2$  nanorods (see Table 1) [78],  $\text{TiO}_2$  mesocrystals (see Table 1) [79], nanosized  $\text{TiO}_2$  (5 C) [80], mesoporous  $\text{TiO}_2$  [81],  $\text{TiO}_2$  nanocrystals [82],  $\text{TiO}_2$  IO (1 C rate) [72],  $\text{TiO}_2$  IO (400 mA/g rate) [71],  $\text{TiO}_2$  IO (10 C rate) [73]. Fig. 3 (a) – (j) are reprinted with permission from [74]. *Inset:* A comparison of the relative capacities from report IO-based  $\text{TiO}_2$  anodes over the first 200 cycles at various C rates, taken for (k).

The impressive performance of the TiO<sub>2</sub> IOs was achieved without the need for binders or conductive additives due to the highly ordered, porous, 3D interconnected structure, which is inherent to the IOs. SEM images demonstrate that the IO structure is retained even after thousands of cycles as shown in Fig. 3g – j. Previous reports for other anode materials such as Si and Ge have shown that volume expansion during long term cycling can lead to substantial capacity fading due to significant changes in nanostructure morphology. [83, 84] However the 3D porous structure of the TiO<sub>2</sub> IOs is retained via expansion of the IO walls into the pores. A comparison of the capacity values reported for the rutile TiO<sub>2</sub> IOs and various other TiO<sub>2</sub> nanostructures, including anatase IO samples is presented in Fig. 3k. SEM images of all the TiO<sub>2</sub> nanostructures in this comparison were shown in Fig. 2. The rutile IO samples outperformed some other TiO<sub>2</sub> nanostructures, particularly in cases where the rates are comparable, demonstrating stable high capacity values over hundreds of cycles. This indicates that rutile TiO<sub>2</sub> IOs are a very promising anode material for Li-ion batteries. The survey concludes that polymorphs of TiO<sub>2</sub> in IO form offer superior performance to various nanostructures or composites of TiO<sub>2</sub>, even at relatively slow and fast rates (see inset to Fig. 3k). Further details can be found in Table 1. We acknowledge that comparisons to other structures and compositions can be limited when different electrodes, salts, specific currents etc. are used in experiments. In our analysis for this short review, we obtained capacity and cycling data, with identified specific currents to compared to IO structured analogues of similar materials.

Material	Phase	C-rate	Charge Capacity mAh/g					Ref.
			50th	100th	200th	500th	1000th	
TiO <sub>2</sub> Inverse Opal	Rutile	75 mA g <sup>-1</sup>	178	168	157	148	138	[74]
TiO <sub>2</sub> Submicroboxes	Rutile	5 C				141		[51]
Nanometer-Sized TiO <sub>2</sub>	Rutile	C/20	160					[76]
TiO <sub>2</sub> Nanoneedles	Rutile	1 C	140					[77]
Porous TiO <sub>2</sub> nanorod microspheres	Rutile	C/5						[78]
TiO <sub>2</sub> mesocrystals	Rutile	1 C		133				[79]
Nanosized TiO <sub>2</sub>	Rutile	5 C		125			105	[80]
Mesoporous TiO <sub>2</sub>	Rutile	1 C		140				[81]
TiO <sub>2</sub> Nanocrystals	Anatase	200 mA/g		110				[82]
TiO <sub>2</sub> Inverse Opal	Anatase	1 C			126			[72]
TiO <sub>2</sub> Inverse Opal	Anatase	400 mA/g			117			[71]

TiO <sub>2</sub> Inverse Opal on Carbon Cloth	Anatase	10 C					111	[73]
---	---------	------	--	--	--	--	-----	------

**Table 1.** Comparison of charge capacities obtained for various rutile and anatase TiO<sub>2</sub> nanostructures from the literature.

### GeO<sub>2</sub> Anode Materials

Germanium dioxide (GeO<sub>2</sub>) is another promising candidate for high-capacity anode electrodes due to its high theoretical capacity (1100 mAh/g). [85] GeO<sub>2</sub> also holds a great deal of potential as an anode material due as a dual storage mechanism material. [84] A recent review by Bresser et al. discussed the development of high energy Li-ion anode materials which target the beneficial combination of conversion and alloying lithium storage mechanisms in a single compound. [86] Consequently, various GeO<sub>2</sub> nanostructures such as nanowires and nanoparticles being investigated as anode materials. [84, 87-89] Initial reports on the electrochemical performance of GeO<sub>2</sub> NPs demonstrated low capacities with limited cycle life, for example GeO<sub>2</sub> NPs reported by Peña et al. suffered from significant capacitive decay from 740 to 225 mAh/g after only 10 cycles, using a slow C-rate of C/20. [90] In contrast to this, GeO<sub>2</sub> NPs reported by Li et al. demonstrated stable capacity retention over 50 cycles at a C-rate of 1 C, achieving capacity values of 940 and 865 after the 10<sup>th</sup> and 50<sup>th</sup> charges. [91] In recent years there is still a large variation in the capacity values reported for GeO<sub>2</sub> based anode materials which are cycled under the same conditions. Mesoporous GeO<sub>2</sub> and GeO<sub>2</sub> microparticles were both cycled galvanostatically using a specific current of 500 mA/g and demonstrated capacity values of ~ 500 and 730 mAh/g after, 50 cycles respectively. [92, 93] Consequently the fabrication of truly reproducible GeO<sub>2</sub> based-electrodes with satisfactory stable cycling and high capacities still presents a big challenge for next generation Li-ion batteries.

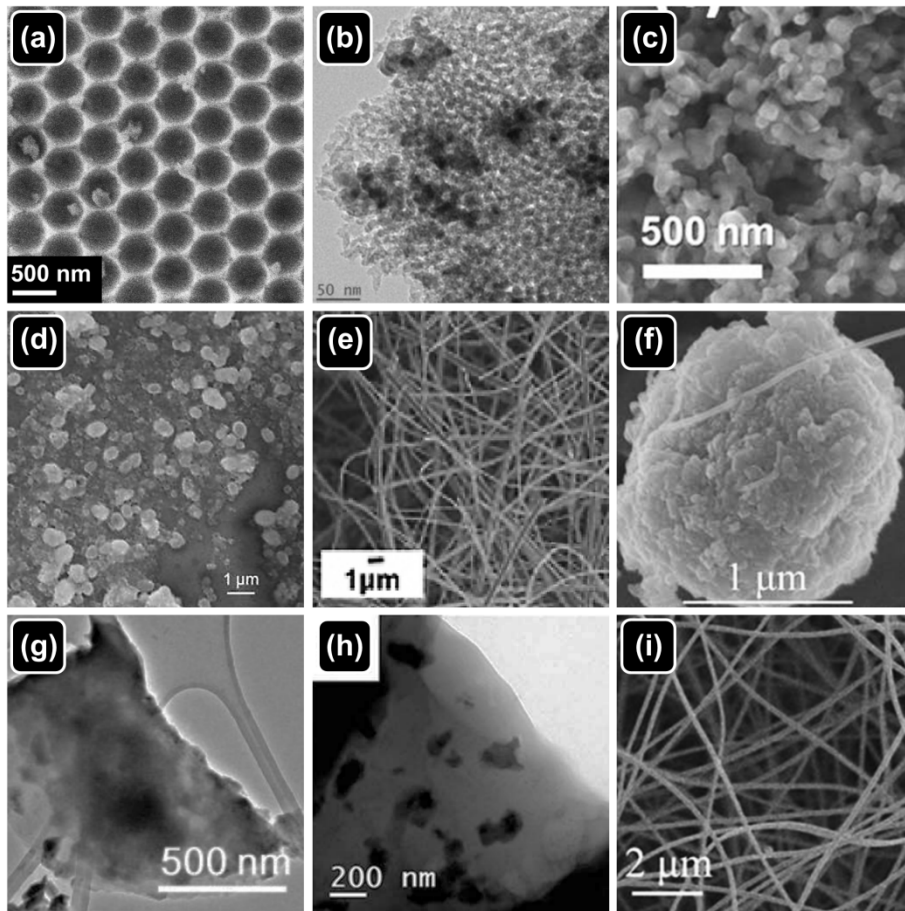


**Fig. 4.** (a) SEM image of a GeO<sub>2</sub> IO [91], (b) TEM image of a GeO<sub>2</sub>/mesoporous carbon composite [92], SEM images of (c) GeO<sub>2</sub> nanoparticles [93], (d) rGO/GeO<sub>2</sub>/PANI composite [94], (e) GeO<sub>2</sub>-C fibers [95] and (f) GeO<sub>x</sub> microspheres [88], TEM images of (g) Ge/C nanocomposite [96] and (h) Ge/C nanocomposite [97], (i) SEM image of Ge/C nanofibers [98].

There are very few papers on the preparation of GeO<sub>2</sub> IOs and they have mainly focused on their optical properties. [94, 95] To date, there has only been one report on their electrochemical performance. [96] We prepared hexagonally ordered GeO<sub>2</sub> IO anode materials by annealing a self-assembled, ordered PS sphere opal template, on stainless steel, infilled with a germanium (IV) ethoxide (Ge(OC<sub>2</sub>H<sub>5</sub>)<sub>4</sub>) precursor solution. The resulting IO samples were highly ordered, porous, crystalline, interconnected networks of GeO<sub>2</sub> as shown in the SEM and TEM images shown in Fig. 5a - c. The TEM image in Fig. 5d demonstrates the GeO<sub>2</sub> NP sub-structure of the IO walls with an average diameter of the NPs of ~25 nm. Galvanostatic cycling of the GeO<sub>2</sub> IOs demonstrated their exceptional capacity retention properties, achieving a reversible capacity of ~ 856 and 714 mAh/g after the 50<sup>th</sup> and 250<sup>th</sup> cycles, respectively when cycled at a specific current of 150 mA/g, as shown in Fig. 5e.

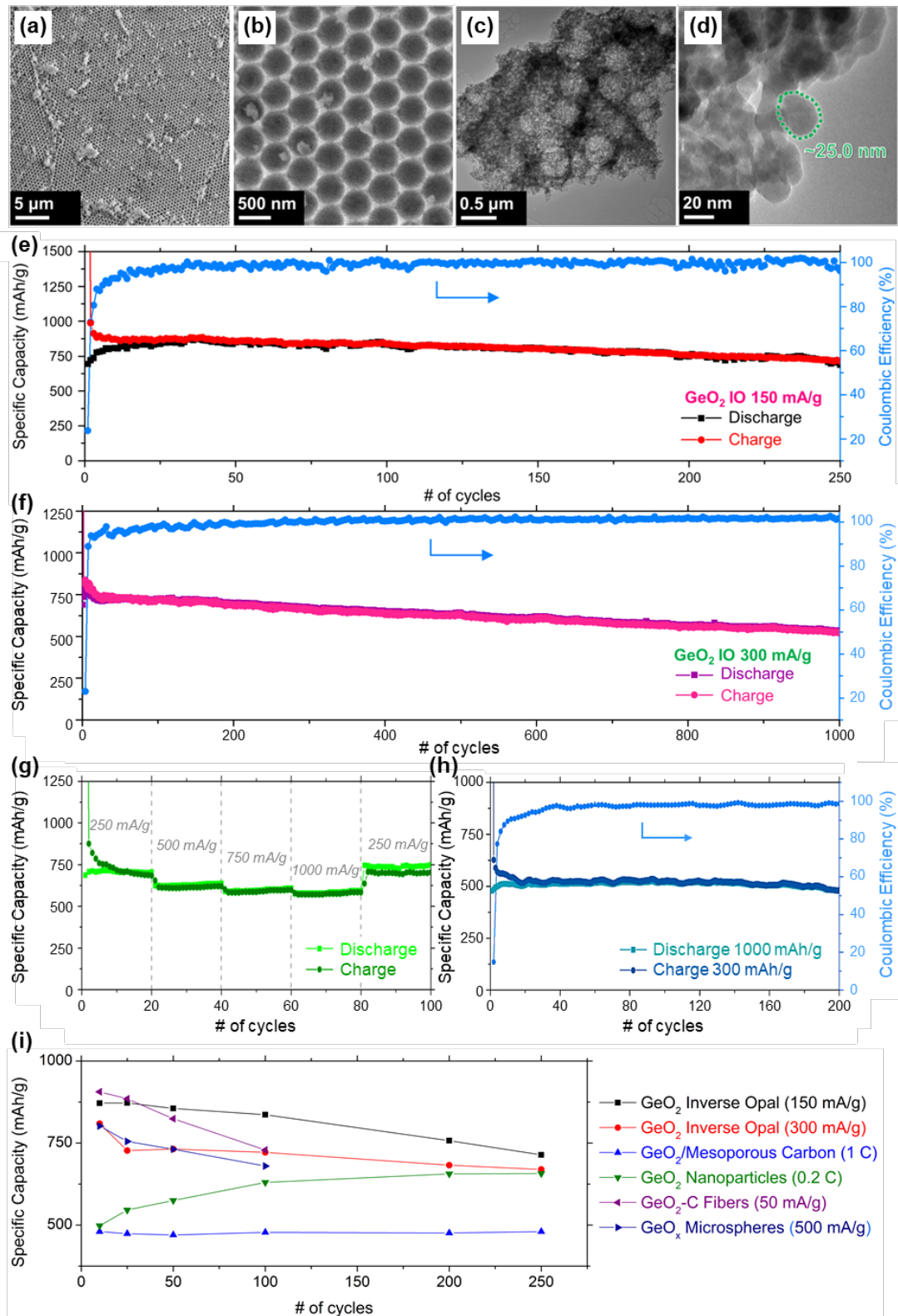


**Fig. 5.** (a) and (b) SEM images of a typical GeO<sub>2</sub> IO anode material. (c) and (d) TEM images showing the walls of the GeO<sub>2</sub> IO materials consist of an agglomeration of crystalline nanoparticles. (e) Specific capacity and coulombic efficiency values obtained for GeO<sub>2</sub> IOs over 250 cycles, at a specific current of 150 mA/g in a potential window of 1.5 – 0.01 V (vs Li/Li<sup>+</sup>). (f) Specific capacity and coulombic efficiency values obtained for GeO<sub>2</sub> IOs over 1000 cycles, at a specific current of 300 mA/g. (g) Rate capability test for a GeO<sub>2</sub> IO over 100 cycles, using specific currents ranging from 250 to 1000 mA/g. (h) Specific capacity and coulombic efficiency values obtained for a GeO<sub>2</sub> IO charged at a specific current of 300 mA/g and discharged at a specific current of 1000 mA/g, in a potential window of 1.50 – 0.01 V (vs Li/Li<sup>+</sup>). (i) Comparison of reported specific capacity values for GeO<sub>2</sub> nanostructures: GeO<sub>2</sub> IO (150 mA/g) [97], GeO<sub>2</sub> IO (300 mA/g) [97], GeO<sub>2</sub>/mesoporous carbon [98], GeO<sub>2</sub> nanoparticles [99], rGO/GeO<sub>2</sub>/PANI [100] (see Table

2), GeO<sub>2</sub>-C fibers [101], GeO<sub>x</sub> microspheres [93], Ge/C nanocomposite (200 mA/g) (see Table 2) [102], Ge/C nanocomposite (200 mA/g) (see Table 2) [103], Ge/C nanofibers (see Table 2) [104].

The long cycle life response of the GeO<sub>2</sub> IOs was determined by galvanostatic cycling with a specific current of 300 mA/g for 1000 cycles. The impressive stability of the GeO<sub>2</sub> IO samples was apparent from the capacity values obtained during cycling. The specific capacities after the 500<sup>th</sup> and 1000<sup>th</sup> cycles were 632 and 521 mAh/g respectively, corresponding to capacity retentions of 76 and 63% from the 2<sup>nd</sup> cycle, as can be seen in Fig. 5f. The ability of the GeO<sub>2</sub> IOs to deliver large reversible capacities when cycled using high specific currents of up to 1 A/g, was demonstrated through rate capability testing. The IO samples exhibited impressive tolerance to cumulatively higher rates with minimal capacity fading, as shown in Fig. 5g. Asymmetric galvanostatic cycling (Fig. 5h) revealed that GeO<sub>2</sub> IOs can deliver large stable capacities (~500 mAh/g) over 200 cycles when discharged with specific current that was >3× the specific current used to charge the anode.

Material	C-rate	Charge Capacity mAh/g					250th	Ref.
		10th	25th	50th	100th	200th		
GeO <sub>2</sub> Inverse Opal	150 mA/g	871.5	872.5	855.6	836.4	757.2	714	[97]
GeO <sub>2</sub> Inverse Opal	300 mA/g	809.3	727.2	731.7	721.6	682.4	669.5	[97]
GeO <sub>2</sub> /Mesoporous Carbon	1 C	480	474	470	478	476	480	[98]
GeO <sub>2</sub> Nanoparticles	0.2 C	498	546	575	630	656	657	[99]
rGO/GeO <sub>2</sub> /PANI	0.1 C	794	768	730	647			[100]
GeO <sub>2</sub> -C Fibers	50 mA/g	906	885	824	729			[101]
GeO <sub>x</sub> Microspheres	500 mA/g	802	755	731	680			[93]
Ge/C Nanocomposite	200 mA/g	673	627	596	540			[102]
Ge/C Nanocomposite	200 mA/g	782	727	685	629			[103]
Ge Nanoparticles/ C Nanofibers	0.15 C	831	811	774	747			[104]

**Table 2.** Comparison of charge capacities obtained for various GeO<sub>2</sub> and some Ge-based materials with various morphologies and at different C-rates from the literature.

The capacity values obtained for the GeO<sub>2</sub> IOs are greater than previously reported values for other GeO<sub>2</sub> nanostructures and comparable to values obtained from pure Ge nanostructures. We surveyed recent papers on GeO<sub>2</sub> anodes, including some composite electrode formulations and compared the rate and cycling data compared to GeO<sub>2</sub> IO anode materials, and the comparison is summarised in the plot in Fig. 5i. SEM and TEM images of the various GeO<sub>2</sub> and Ge nanostructures which are compared electrochemically are shown in Fig. 4. As was the case for the rutile TiO<sub>2</sub> IOs, the impressive electrochemical performance of the GeO<sub>2</sub> IO

samples was achieved in the absence of any binders or conductive additives, and full details can be found in Ref. [97]. There are numerous reasons for the enhanced performance of the GeO<sub>2</sub> IOs compared to other GeO<sub>2</sub> nanostructures. The large surface area and the high level of porosity provide continuous transport paths for Li ions through the active phase (walls) and the electrolyte phase (pores)[10, 20, 32], while the reversible alloying reactions maintain anode phase that does not appreciably affect electronic conductivity or electrode resistance in the absence of conductive additives. A significant advantage of GeO<sub>2</sub> IOs over other germanium based nanostructured anodes is that they can be prepared without the need for an inert atmosphere or any additional processing steps, such as the preparation of a slurry, and can produce capacity values and retention greater than other GeO<sub>2</sub> nanostructures and comparable to pure Ge-based materials or indeed composites of these materials.

## **Conclusions and outlook**

In this short review, we have looked at recent results on nanoscale materials and assemblies of materials for Li-ion battery anodes, focusing on abundant, voltage-stable and high-capacity anode materials of metal oxides that do not cycle via conversion mode processes. TiO<sub>2</sub> in various crystalline polymorphs and structures, and GeO<sub>2</sub> materials have been shown to be promising as Li-ion battery anodes, and can often be made and scaled up in large quantities using relatively simpler processes. This is particularly true for GeO<sub>2</sub>, which is believed to undergo reduction to a Ge phase prior to lithiation in tandem with SEI formation, and readily cycles with high capacity and high coulombic efficiency. The benefits of introducing porosity are clear, as they ensure that all the active material is electrochemically reduced to the alloying Ge phase, while in other materials, solution and solid state ionic diffusion is enhanced, without kinetic hindrance from polymeric binders. One proviso is that interconnectivity is maintained and material conductivity in the lithiated (crystalline or amorphous) phases is not adversely affected.

Some recent reports have shown that 3D macroporous structure can also accommodate active material in thin film form as a coating on a metallic current collector that is itself, structured as an inverse opal. Although gravimetric energy densities are limited from the thin coating of active material and the density of the underlying current collector, the approach did prove that short diffusivity limitation could be mitigated by

using conformal thin film electrode coating, with ionic diffusivity of cations in the electrolyte reduced somewhat by soakage into the inverse opal structure. Involving the structure of the current collector is a nice way to address the kinetics directly, which minimizing large changes to overall electrode conductivity, which is critical for some materials once alloyed, intercalated or lithiated to amorphous or insulating phases. Our approach has been to use abundant materials with phases and methods of growth on current collectors that ensures that gravimetric energy density concerns are limited as much as possible. We do this by ensure the only material on the electrode is the active material, and that it maintains its 3D open-worked IO structure during long term cycling. Not all materials, we believe, will behave this way, but it remains to be seen if the porosity, interconnectivity, or the order of the porosity is the most important factor in the improved long-term cycling response of efficiently reversible, non-conversion mode metal oxide anodes for Li-ion or emerging alternative cation intercalation anodes for batteries.

## **Acknowledgements**

This work was also supported by Science Foundation Ireland (SFI) through an SFI Technology Innovation and Development Award under contract no. 13/TIDA/E2761. This publication has also emanated from research supported in part by a research grant from SFI under Grant Number 14/IA/2581. We acknowledge support from the Irish Research Council Government of Ireland Award under GOIPG/2016/946.

## References

- [1] S. Oyama, "Strong Growth to Drive Lithium-ion Battery Market to \$61 Billion by 2020 - Rechargeable Batteries Special Report" IHS (2011).
- [2] Rechargeable Batteries for Consumer Products, Frost and Sullivan (2010).
- [3] J.M. Tarascon, M. Armand, *Nature* **414** (2001) 359.
- [4] J.B. Goodenough, Y. Kim, *Chem. Mater.* **22** (2010) 587.
- [5] B. Scrosati, J. Garche, *J. Power Sources* **195** (2010) (9) 2419.
- [6] G.R. Fleming, M.A. Ratner, *Phys. Today* **61** (2008) 28.
- [7] J.H. Pikul, H.G. Zhang, J. Cho, P.V. Braun, W.P. King, *Nat. Commun.* **4** (2013) 1732.
- [8] J.C. Lytle, In: Y. Abu-Lebdeh, I. Davidson, Editors, *Nanotechnology for Lithium-Ion Batteries*, Springer Science+Business Media, LLC (2013).
- [9] D. McNulty, D.N. Buckley, C. O'Dwyer, *J. Power Sources* **267** (2014) 831.
- [10] M. Osiak, H. Geaney, E. Armstrong, C. O'Dwyer, *J. Mater. Chem. A* **2** (2014) 9433.
- [11] G.A. Nazri, G. Pistoia, *Lithium Batteries: Science and Technology*, Kluwer Academic/Plenum (2004).
- [12] C. O'Dwyer, *Nano – The Magazine for Small Science* (February 2010) (Issue 16).
- [13] *BBC News* (<http://www.bbc.co.uk/news/technology-22191650> (2013)) (17 April).
- [14] H. Zhang, X. Yu, P.V. Braun, *Nat. Nanotechnol.* **6** (2011) 277.
- [15] C. O'Dwyer, *Adv. Mater.* **28** (2016) 5681.
- [16] P.V. Braun, *Chem. Mater.* **26** (2013) 277.
- [17] E. Armstrong, W. Khunsin, M. Osiak, C.M.S. Torres, C. O'Dwyer, *ECS Trans.* **58** (2014) (47) 9.
- [18] H. Zhang, P.V. Braun, *Nano Lett.* **12** (2012) (6) 2778.
- [19] X. Li, A. Dhanabalan, L. Gu, C. Wang, *Adv. Energy Mater.* **2** (2012) (2) 238.
- [20] A.S. Arico, P. Bruce, B. Scrosati, J.M. Tarascon, W.V. Schalkwijk, *Nat. Mater.* **4** (2005) 366.
- [21] N. Li, C.R. Martin, B. Scrosati, *J. Power Sources* **97–98** (2001) 240.
- [22] L. Mishchenko, B. Hatton, M. Kolle, J. Aizenberg, *Small* **8** (2012) 1904.
- [23] B. Luo, B. Wang, X. Li, Y. Jia, M. Liang, L. Zhi, *Adv. Mater.* **24** (2012) 3538.
- [24] D.-Y. Kang, S.-O. Kim, Y.J. Chae, J.K. Lee, J.H. Moon, *Langmuir* **29** (2013) (4) 1192.
- [25] W. McSweeney, O. Lotty, N.V.V. Mogili, C. Glynn, H. Geaney, D. Tanner, J.D. Holmes, C. O'Dwyer, *J. Appl. Phys.* **114** (2013) 034309.
- [26] N.S. Ergang, J.C. Lytle, K.T. Lee, S.M. Oh, W.H. Smyrl, A. Stein, *Adv. Mater.* **18** (2006) 1750.
- [27] N.S. Ergang, M.A. Fierke, Z. Wang, W.H. Smyrl, A. Stein, *J. Electrochem. Soc.* **154** (2007) A1135.
- [28] Z. Wang, M.A. Fierke, A. Stein, *J. Electrochem. Soc.* **155** (2008) A658.
- [29] N.S. Ergang, J.C. Lytle, H.W. Yan, A. Stein, *J. Electrochem. Soc.* **152** (2005) A1989.
- [30] A. Stein, B.E. Wilson, S.G. Rudisill, *Chem. Soc. Rev.* **42** (2013) 2763.
- [31] J.S. Sakamoto, B. Dunn, *J. Mater. Chem.* **12** (2002) 2859.
- [32] J.W. Long, B. Dunn, D.R. Rolison, H.S. White, *Chem. Rev.* **104** (2004) 4463.
- [33] D.R. Rolison, *Chem. Soc. Rev.* **38** (2009) 226.
- [34] P.G. Bruce, B. Scrosati, J.M. Tarascon, *Angew. Chem. Int. Ed.* **47** (2008) 2930.
- [35] M. Fittipaldi, V. Gombac, A. Gasparotto, C. Deiana, G. Adami, D. Barreca, T. Montini, G. Martra, D. Gatteschi, P. Fornasiero, *ChemPhysChem* **12** (2011) (12) 2221.
- [36] J. Balbuena, G. Carraro, M. Cruz, A. Gasparotto, C. Maccato, A. Pastor, C. Sada, D. Barreca, L. Sanchez, *RSC Advances* **6** (2016) (78) 74878.
- [37] J. Bai, B. Zhou, *Chem. Rev.* **114** (2014) (19) 10131.
- [38] V. Galstyan, E. Comini, G. Faglia, G. Sberveglieri, *Sensors* **13** (2013) (11) 14813.
- [39] Y. Liang, Y. Li, H. Wang, H. Dai, *J. Am. Chem. Soc.* **135** (2013) (6) 2013.
- [40] Y. Yan, Q. Liu, X. Du, J. Qian, H. Mao, K. Wang, *Anal. Chim. Acta* **853** (2015) 258.
- [41] S. Wu, Z. Weng, X. Liu, K.W.K. Yeung, P.K. Chu, *Adv. Func. Mater.* **24** (2014) (35) 5464.
- [42] Q. Zhou, Z. Fang, J. Li, M. Wang, *Microporous Mesoporous Mater.* **202** (2015) 22.
- [43] G. Wang, H. Wang, Y. Ling, Y. Tang, X. Yang, R.C. Fitzmorris, C. Wang, J.Z. Zhang, Y. Li, *Nano Lett.* **11** (2011) (7) 3026.
- [44] I.S. Cho, Z. Chen, A.J. Forman, D.R. Kim, P.M. Rao, T.F. Jaramillo, X. Zheng, *Nano Lett.* **11** (2011) (11) 4978.

- [45] G. Jiang, Z. Lin, C. Chen, L. Zhu, Q. Chang, N. Wang, W. Wei, H. Tang, *Carbon* **49** (2011) (8) 2693.
- [46] G. Lui, J.-Y. Liao, A. Duan, Z. Zhang, M. Fowler, A. Yu, *J. Mater. Chem. A* **1** (2013) (39) 12255.
- [47] Y. Zhang, Y. Tang, W. Li, X. Chen, *ChemNanoMat* **2** (2016) (8) 764.
- [48] D. Barreca, G. Carraro, A. Gasparotto, C. Maccato, M. Cruz-Yusta, J.L. Gómez-Camer, J. Morales, C. Sada, L. Sánchez, *ACS Applied Materials & Interfaces* **4** (2012) (7) 3610.
- [49] Y. Tang, Y. Zhang, J. Deng, J. Wei, H.L. Tam, B.K. Chandran, Z. Dong, Z. Chen, X. Chen, *Adv. Mater.* **26** (2014) (35) 6111.
- [50] J. Zheng, L. Liu, G. Ji, Q. Yang, L. Zheng, J. Zhang, *ACS Appl. Mater. Interfaces* **8** (2016) (31) 20074.
- [51] X.-Y. Yu, H.B. Wu, L. Yu, F.-X. Ma, X.W. Lou, *Angew. Chem. Int. Ed.* **54** (2015) (13) 4001.
- [52] H. Liu, W. Li, D. Shen, D. Zhao, G. Wang, *J. Am. Chem. Soc.* **137** (2015) (40) 13161.
- [53] M.-C. Yang, Y.-Y. Lee, B. Xu, K. Powers, Y.S. Meng, *J. Power Sources* **207** (2012) 166.
- [54] M. Zhen, X. Guo, G. Gao, Z. Zhou, L. Liu, *Chem. Commun.* **50** (2014) (80) 11915.
- [55] O. Rhee, G. Lee, J. Choi, *ACS Appl. Mater. Interfaces* **8** (2016) (23) 14558.
- [56] R. Mo, Z. Lei, K. Sun, D. Rooney, *Adv. Mater.* **26** (2014) (13) 2084.
- [57] B. Wang, H. Xin, X. Li, J. Cheng, G. Yang, F. Nie, **4** (2014) 3729.
- [58] J. Song, B. Sun, H. Liu, Z. Ma, Z. Chen, G. Shao, G. Wang, *ACS Appl. Mater. Interfaces* **8** (2016) (24) 15225.
- [59] G. Collins, E. Armstrong, D. McNulty, S. O'Hanlon, H. Geaney, C. O'Dwyer, *Sci. Tech. Adv. Mater.* **17** (2016) (1) 563.
- [60] E. Armstrong, D. McNulty, H. Geaney, C. O'Dwyer, *ACS Appl. Mater. Interfaces* **7** (2015) (48) 27006.
- [61] D. McNulty, H. Geaney, E. Armstrong, C. O'Dwyer, *J. Mater. Chem. A* **4** (2016) (12) 4448.
- [62] D. McNulty, H. Geaney, C. O'Dwyer, *Sci. Rep.* **7** (2017) 42263.
- [63] David McNulty, H. Geaney, E. Carroll, S. Garvey, A. Lonergan, C. O'Dwyer, *Mater. Res. Express* **4** (2017) (2) 025011.
- [64] A. Vu, Y. Qian, A. Stein, *Adv. Energy Mater.* **2** (2012) (9) 1056.
- [65] J.H. Pikul, H.G. Zhang, J. Cho, P.V. Braun, W.P. King, *Nat. Commun.* **4** (2013) 1732.
- [66] H. Zhang, X. Yu, P.V. Braun, *Nat. Nanotechnol.* **6** (2011) (5) 277.
- [67] L. Kavan, M. Zúkalová, M. Kalbáč, M. Graetzel, *J. Electrochem. Soc.* **151** (2004) (8) A1301.
- [68] M.D. Bhatt, C. O'Dwyer, *Phys. Chem. Chem. Phys.* **17** (2015) 4799.
- [69] I. Nam, J. Park, S. Park, S. Bae, Y.G. Yoo, J.W. Han, J. Yi, *Phys. Chem. Chem. Phys.* **29** (2017) 13140.
- [70] H. Kim, M.G. Kim, J. Cho, *Adv. Energy Mater.* **2** (2012) (12) 1425.
- [71] H. Jiang, X. Yang, C. Chen, Y. Zhu, C. Li, *New J. Chem.* **37** (2013) (5) 1578.
- [72] J. Jin, S.-Z. Huang, J. Liu, Y. Li, D.-S. Chen, H.-E. Wang, Y. Yu, L.-H. Chen, B.-L. Su, *J. Mater. Chem. A* **2** (2014) (25) 9699.
- [73] G. Lui, G. Li, X. Wang, G. Jiang, E. Lin, M. Fowler, A. Yu, Z. Chen, *Nano Energy* **24** (2016) 72.
- [74] D. McNulty, E. Carroll, C. O'Dwyer, *Adv. Energy Mater.* **7** (2017) (12) 1602291.
- [75] R. Su, R. Bechstein, L. Sør, R.T. Vang, M. Sillassen, B. Esbjörnsson, A. Palmqvist, F. Besenbacher, *J. Phys. Chem. C* **115** (2011) (49) 24287.
- [76] Y.S. Hu, L. Kienle, Y.G. Guo, J. Maier, *Adv. Mater.* **18** (2006) (11) 1421.
- [77] Y. Gan, L. Zhu, H. Qin, Y. Xia, H. Xiao, L. Xu, L. Ruan, C. Liang, X. Tao, H. Huang, W. Zhang, *Solid State Ion.* **269** (2015) 44.
- [78] H. Qiao, Y. Wang, L. Xiao, L. Zhang, *Electrochem. Commun.* **10** (2008) (9) 1280.
- [79] Z. Hong, M. Wei, T. Lan, G. Cao, *Nano Energy* **1** (2012) (3) 466.
- [80] M. Pfanzelt, P. Kubiak, M. Wohlfahrt-Mehrens, *Electrochem. Solid State Lett.* **13** (2010) (7) A91.
- [81] D. Wang, D. Choi, Z. Yang, V.V. Viswanathan, Z. Nie, C. Wang, Y. Song, J.-G. Zhang, J. Liu, *Chem. Mater.* **20** (2008) (10) 3435.
- [82] Z. Zhang, L. Zhang, W. Li, A. Yu, P. Wu, *ACS Appl. Mater. Interfaces* **7** (2015) (19) 10395.
- [83] M.T. McDowell, S.W. Lee, W.D. Nix, Y. Cui, *Adv. Mater.* **25** (2013) (36) 4966.
- [84] Z. Hu, S. Zhang, C. Zhang, G. Cui, *Coord. Chem. Rev.* **326** (2016) 34.
- [85] J.K. Feng, M.O. Lai, L. Lu, *Electrochim. Acta* **62** (2012) 103.
- [86] D. Bresser, S. Passerini, B. Scrosati, *Energy Environ. Sci.* **9** (2016) (11) 3348.
- [87] C.K. Chan, X.F. Zhang, Y. Cui, *Nano Lett.* **8** (2008) (1) 307.

- [88] D.-J. Xue, S. Xin, Y. Yan, K.-C. Jiang, Y.-X. Yin, Y.-G. Guo, L.-J. Wan, *J. Am. Chem. Soc.* **134** (2012) (5) 2512.
- [89] X. Xiao, X. Li, S. Zheng, J. Shao, H. Xue, H. Pang, *Adv. Mater. Inter.* **4** (2017) (6) 1600798.
- [90] J.S. Peña, I. Sandu, O. Joubert, F.S. Pascual, C.O. Areán, T. Brousse, *Electrochem. Solid State Lett.* **7** (2004) (9) A278.
- [91] G.-A. Li, W.-C. Li, W.-C. Chang, H.-Y. Tuan, *RSC Adv.* **6** (2016) (101) 98632.
- [92] J. Hwang, C. Jo, M.G. Kim, J. Chun, E. Lim, S. Kim, S. Jeong, Y. Kim, J. Lee, *ACS Nano* **9** (2015) (5) 5299.
- [93] W. He, H. Tian, X. Wang, F. Xin, W. Han, *J. Mater. Chem. A* **3** (2015) (38) 19393.
- [94] X. Meng, R. Al-Salman, J. Zhao, N. Borissenko, Y. Li, F. Endres, *Angew. Chem. Int. Ed.* **48** (2009) (15) 2703.
- [95] X. Meng, J. Zhao, H. Li, F. Endres, Y. Li, *Opt. Express* **20** (2012) (9) 9421.
- [96] D. McNulty, C. O'Dwyer, *Electrochem. Soc. Meeting Abstracts MA2017-01* (2017) (5) 352.
- [97] D. McNulty, H. Geaney, D. Buckley, C. O'Dwyer, *Nano Energy* (2017).
- [98] A. Jahel, A. Darwiche, C. Matei Ghimbeu, C. Vix-Guterl, L. Monconduit, *J. Power Sources* **269** (2014) 755.
- [99] Y.-M. Lin, K.C. Klavetter, A. Heller, C.B. Mullins, *J. Phys. Chem. Lett.* **4** (2013) (6) 999.
- [100] S. Sarkar, R. Borah, A.L. Santhosha, R. Dhanya, C. Narayana, A.J. Bhattacharyya, S.C. Peter, *J. Power Sources* **306** (2016) 791.
- [101] Q. Yang, T. Sun, J.-Y. Yu, J.-X. Ma, *Chin. Chem. Lett.* **27** (2016) (3) 412.
- [102] W. Guo, L. Mei, Q. Feng, J. Ma, *Mater. Chem. Phys.* **168** (2015) 6.
- [103] H.-S. Choe, S.-J. Kim, M.-C. Kim, D.-M. Kim, G.-H. Lee, S.-B. Han, D.-H. Kwak, K.-W. Park, *RSC Adv.* **6** (2016) (77) 72926.
- [104] W. Li, Z. Yang, J. Cheng, X. Zhong, L. Gu, Y. Yu, *Nanoscale* **6** (2014) (9) 4532.